

Thermodynamic conditions during growth determine the magnetic anisotropy in epitaxial thin-films of $\text{La}_{0.7}\text{Sr}_{0.3}\text{MnO}_3$.

J. M. Vila-Fungueiriño,¹ Cong Tinh Bui,¹ B. Rivas-Murias,¹ E. Winkler,² J. Milano,² J. Santiso,³ and F. Rivadulla^{1,*}

¹*Center for Research in Biological Chemistry and Molecular Materials (CIQUS),
University of Santiago de Compostela, 15782 Santiago de Compostela, Spain*

²*Centro Atómico Bariloche, CNEA-CONICET, 8400 S.C. de Bariloche, Río Negro, Argentina*

³*Catalan Institute of Nanoscience and Nanotechnology (ICN2),
CSIC and The Barcelona Institute of Science and Technology,
Campus UAB, Bellaterra, 08193 Barcelona, Spain*

(Dated: April 5, 2022)

The suitability of a particular material for use in magnetic devices is determined by the process of magnetization reversal/relaxation, which in turn depends on the magnetic anisotropy. Therefore, designing new ways to control magnetic anisotropy in technologically important materials is highly desirable. Here we show that magnetic anisotropy of epitaxial thin-films of half-metallic ferromagnet $\text{La}_{0.7}\text{Sr}_{0.3}\text{MnO}_3$ (LSMO) is determined by the proximity to thermodynamic equilibrium conditions during growth. We performed a series of X-ray diffraction and ferromagnetic resonance (FMR) experiments in two different sets of samples: the first corresponds to LSMO thin-films deposited under tensile strain on (001) SrTiO_3 by Pulsed Laser Deposition (PLD; far from thermodynamic equilibrium); the second were deposited by a slow Chemical Solution Deposition (CSD) method, under quasi-equilibrium conditions. Thin films prepared by PLD show a in-plane cubic anisotropy with an overimposed uniaxial term. A large anisotropy constant perpendicular to the film plane was also observed in these films. However, the uniaxial anisotropy is completely suppressed in the CSD films. The out of plane anisotropy is also reduced, resulting in a much stronger in plane cubic anisotropy in the chemically synthesized films. This change is due to a different rotation pattern of MnO_6 octahedra to accommodate epitaxial strain, which depends not only on the amount of tensile stress imposed by the STO substrate, but also on the growth conditions. Our results demonstrate that the nature and magnitude of the magnetic anisotropy in LSMO can be tuned by the thermodynamic parameters during thin-film deposition.

PACS numbers:

I. INTRODUCTION

Recent developments in thin-film growth showed the enormous potential of epitaxial stress to tune the properties of thin films at a very fundamental level. In perovskite oxides, ABO_3 , strain accommodation occurs through a complex rotation and deformation of corner sharing BO_6 octahedra^{1–3}. This changes the delicate balance of bond-distances and angles and therefore the relative orbital occupation supporting a given magnetic or electrical interaction^{4–10}. Interfacial phenomena like heterogeneous catalysis reactions¹¹, and electronic reconstructions occurring at functional interfaces¹², are also influenced by these effects.

An interesting example given its scientific relevance is the case of half-metallic ferromagnet $\text{La}_{0.7}\text{Sr}_{0.3}\text{MnO}_3$ (LSMO). Growing epitaxial LSMO on cubic (001) SrTiO_3 (STO) results in an orthorhombic (with a monoclinic distortion) unit cell of the magnetic oxide^{1,13}. Biaxial tensile stress ($a=b>c$) imposed by the cubic substrate to the incommensurate rhombohedral lattice of bulk LSMO induces an equal in-(out-) phase rotation of the MnO_6 octahedra along the a -(b -) axis, and no rotation along the c -axis ($a^+a^-c^0$ in the Glazer notation¹⁴). Sandiunenge et al.³ proposed a complex relaxation pattern in which several phases with different symmetry can be distinguished in epitaxial LSMO below 25 nm. These au-

thors identified a critical thickness ≈ 2 nm for the build up of a shear strain field, which induces a rhombohedral twined structure and a progressive compression of the c -axis up to ≈ 10 nm. Beyond this thickness, an elastic deformation of the lattice without any perturbation of the octahedral tilting sets up to ≈ 25 nm. Vailionis et al.¹⁵ confirmed that the mechanism of strain relaxation changes along the film thickness, due to a combined effect of symmetry mismatch close to the interface, and lattice mismatch in the "bulk" of the film. They showed that in the first \approx two unit cells, stress suppresses octahedral rotations and expands the c -axis parameter; farther away from the interface, tilting of MnO_6 octahedra reduce the c -axis parameter consistent with in-plane tensile strain.

An important question is whether this complex relaxation pattern is intrinsic to the accommodation of biaxial tensile stress in LSMO, or if it can be modified by growing the films under very different conditions, thus allowing the system to explore different relaxation paths. After all, previous studies were performed on samples synthesized by PLD and sputtering, far from thermodynamic equilibrium. Here we describe a comparative X-ray diffraction (XRD) and Ferromagnetic resonance (FMR) study of LSMO thin films deposited on STO by Pulsed Laser Deposition (PLD; far from thermodynamic equilibrium), and by a slow chemical deposition method (CSD; close to thermodynamic equilibrium). Our results

demonstrate that magnetic anisotropy in LSMO depends on the conditions during film growth. As a result, a different pattern of rotation of MnO_6 octahedra is accommodated in epitaxial films synthesized by CSD.

II. EXPERIMENTAL DETAILS

Thin films of LSMO of different thicknesses were grown on (001) TiO_2 -terminated SrTiO_3 (STO) substrates. For the PLD films we used an excimer laser (F-Kr, 248 nm) operating at 5 Hz and a fluence of 0.8 J/cm^2 . The films were deposited at 800°C and 200 mTorr of O_2 . For chemically grown films (CSD), a precursor solution was spin-coated on similar substrates, and annealed at high temperature, as described in¹⁶. The thickness of both type of films was determined by X-ray reflectivity and TEM analysis of cross-section lamellae. X-band ($\omega/2\pi \sim 9.4 \text{ GHz}$) FMR experiments were performed in a Bruker-X spectrometer at different temperatures, with the magnetic field applied rotating parallel to the film-plane.

III. RESULTS AND DISCUSSION

In Figure 1 we show a summary of structural results representative of the quality of the samples studied in this work. X-ray reciprocal space maps (RSM) around the (103) reflection of the perovskite for $\approx 20 \text{ nm}$ thick films show that they grow with in-plane lattice parameters well matched to the STO substrate, and without evidence of lattice relaxation (Figure 1a, c)). This is true for every film studied in this work, irrespective of the thickness or the deposition method (CSD or PLD). A high-resolution cross-section TEM image of a thin film of LSMO synthesized by CSD is shown in Figure 1b). The image is representative of the good crystalline quality and abrupt interfaces of all the CSD films reported in this work.

The dependence of the lattice parameters on the thickness is shown in Figure 1d). The c -axis length shows a non-monotonic dependence with the film thickness, passing through a minimum between 10 and 15 nm. Similar behavior was previously reported by Sandiumenge et al.³ for LSMO films synthesized by rf-sputtering. These authors suggested that t_m marks a crossover from a monoclinic to a homogeneously strained rhombohedral phase. Our results show that the existence of this minimum occurs for PLD and CSD samples, therefore suggesting a universal relaxation mechanism depending only on the total strain imposed by the substrate. However, the incommensurability of rhombohedral LSMO to the cubic (001) surface of STO has been suggested to result in an orthorhombic symmetry with a monoclinic distortion ($P2_1/m$)¹³. In order to identify the crystal structure in our films, we have performed a careful XRD analysis around different half order reflections. ($H/2$, $K/2$, $L/2$) reflections are characteristic of a monoclinic or tri-

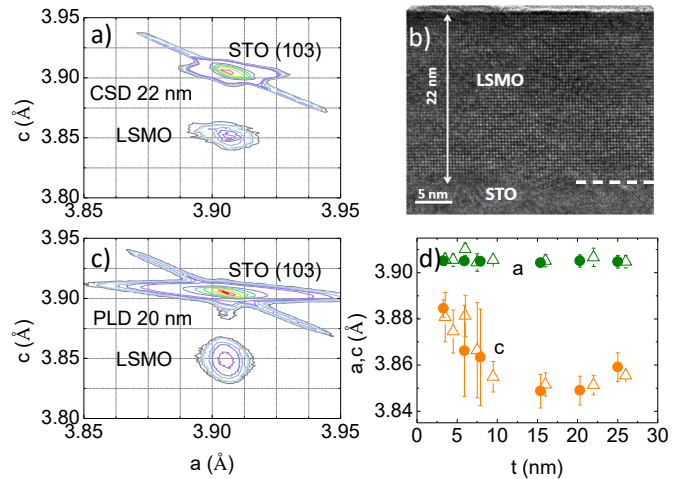


FIG. 1: X-ray maps around the (103) Bragg reflection of the perovskite for two LSMO thin-films deposited on STO by CSD (a) and PLD (c). TEM image of a cross-section lamella of a LSMO thin-film synthesized by CSD (b). The evolution of lattice parameters for several samples of different thicknesses are shown in (d).

clinic symmetry, with $H=K=L$ being an extinction for the rhombohedral R-3C group. For the 20 nm thick sample prepared by PLD, we observed a clear signal around the $(1/2, 1/2, 1/2)$ and $(1/2, 1/2, 3/2)$ reflections, as shown in Figure 2. These are consistent with a rhombohedral (R-3c) phase, with a monoclinic distortion. Although the $(1/2, 0, 1)$ and $(1, 0, 1/2)$ reflections have not been observed in our films, an orthorhombic phase cannot be completely discarded due to the small intensity characteristic of these reflections, particularly in thin-films. On the other hand, half order reflections at $L=3/2$ and absence at $L=1/2$ in films prepared by CSD are consistent with a dominant rhombohedral (R-3c) phase. Also, from the analysis of in-plane (200) and (110) peaks, a fully structural coherence with the substrate is observed along the whole thickness of the films prepared by CSD (see Figure 3). No satellites peaks or diffuse scattering associated to twinnings or strong mosaicity are observed in these samples.

Given the equal in-plane tensile stress imposed by the substrate along the a/b directions, these structural results therefore suggest a different rotation pattern of the MnO_6 octahedra to accommodate the tensile stress in samples synthesized by CSD with respect to PLD. We want to remark that this result is reproducible in different samples prepared from CSD under similar conditions.

The structural difference reported in Figure 2 is also manifested in the magnetic properties of the CSD and PLD films (see Figure 4). The magnetic moment at saturation and the Curie temperature (T_c) of $\approx 20 \text{ nm}$ thick films are close to the bulk values (590 emu/cm^3 and 350 K) and are very similar in both sets of samples, discarding any significant variation in their stoichiometry.

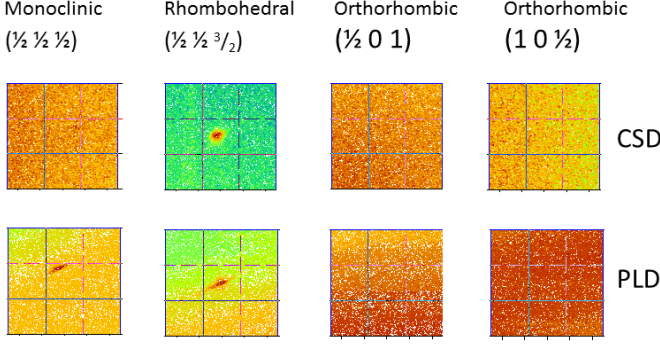


FIG. 2: Half-order Bragg reflections for thin films prepared by CSD (22 nm, top) and PLD (20 nm, bottom) respectively. Different reflections characteristic of different crystallographic phases are analyzed.

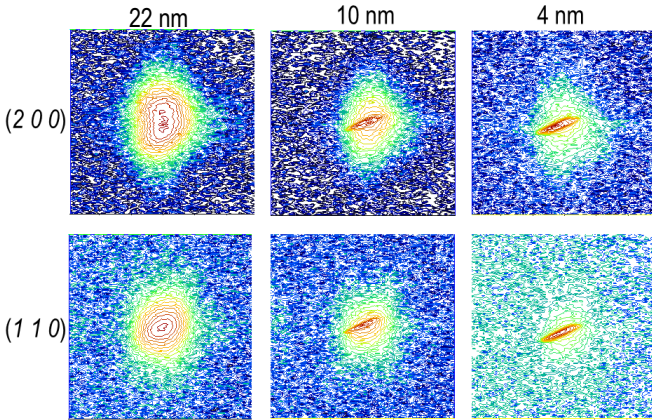


FIG. 3: In plane (200) and (110) Bragg reflections for thin films of LSMO prepared by CSD, with different thickness.

However, the coercive field (H_c) shows a completely different behavior: while the samples synthesized by PLD show a very small, bulk-like, $H_c \approx 50$ -100 Oe, it increases by an order of magnitude in the films synthesized by CSD. Therefore, the change in H_c probably implies different magnetocrystalline anisotropy between the CSD and PLD films. This could be due to differences in the strength of Mn-O-Mn exchange interactions along different directions of the crystal, as a result of the structural differences identified before. However, to give a definitive proof of this subtle structural distortion in thin-films prepared by different methods is very challenging using conventional laboratory XRD equipment.

To avoid this difficulty, the evolution of the structural

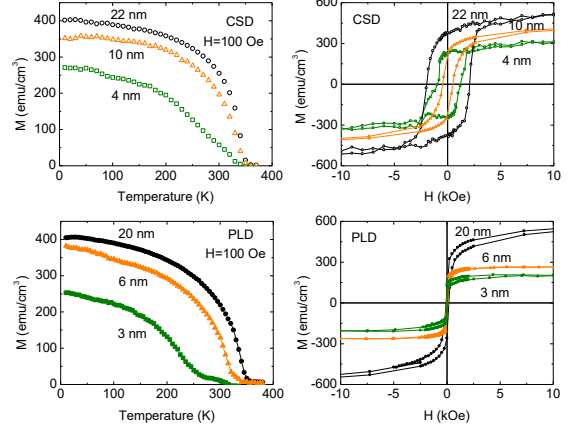


FIG. 4: Temperature and field dependence (at 10 K) of the magnetization for CSD (top) and PLD (bottom) thin films. The hysteresis loops were measured at 10 K with the magnetic field in the film plane along the (100) axis of STO. Saturation of the magnetization occurs at $H < 1.5$ T.

parameters with thickness was studied indirectly by ferromagnetic resonance. FMR is a technique very sensitive to small variations in the magnitude of the different magnetic anisotropy terms. Different rotation patterns of the MnO_6 octahedra along different directions of the crystal will change the orbital overlap and, through spin-orbit coupling also change the magnetocrystalline anisotropy of the films. We will show that these changes measured by FMR can be correlated with the structural distortions in the films.

The angular dependence of the resonance field (H_r) in a FMR experiment can be evaluated at the magnetization equilibrium angles, θ_0 and ϕ_0 for the different orientation of the magnetic field¹⁷:

$$\left(\frac{\omega}{\gamma}\right)^2 = \frac{1}{M^2 \sin^2 \theta} \left[\frac{\partial^2 F}{\partial \theta^2} \frac{\partial^2 F}{\partial \phi^2} - \left(\frac{\partial^2 F}{\partial \theta \partial \phi} \right)^2 \right]_{\theta_0, \phi_0} \quad (1)$$

where ω is the angular frequency, M is the saturation magnetization, F is the free energy of the system and $\gamma = g\mu_B/\hbar$, where g is the gyromagnetic factor and μ_B is the Bohr magneton. Based on the structural results, three different anisotropy terms were included in the free energy expression: a biaxial in plane anisotropy constant K_4^{IP} , an in plane uniaxial anisotropy constant K_u , and a perpendicular out of plane anisotropy constant K_{out} along $[001]$ ¹⁸:

$$F = -\mu_0 \mathbf{H} \cdot \mathbf{M} + \frac{\mu_0}{2} M^2 \cos^2 \theta - \frac{K_4^{IP}}{4} \sin^4 \theta \sin^2 2\phi - K_{out} \cos^2 \theta + K_u \sin^2 \theta \cos^2(\phi - \frac{\pi}{4}) \quad (2)$$

where the first and second terms correspond to the Zeeman and demagnetization energy, respectively. The

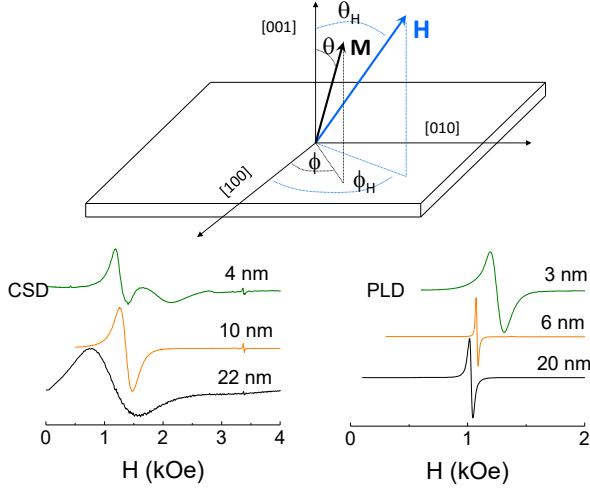


FIG. 5: Top: Scheme of the coordinate system used in Eq.1 and 2 related to the crystal axis of the STO substrate. Bottom: FMR lines for thin-films of LSMO of different thickness, synthesized by CSD (left) and PLD (right). The experiments were performed at 200 K.

vacuum permeability is given by μ_0 , and θ and ϕ are the polar and azimuthal angles of the magnetization vector, according to the scheme of Figure 5. In this way the values of K_4^{IP} , K_u , and K_{out} can be determined from fittings of experimental $H_r(\theta, \phi)$ curves by solving self-consistently Eq. (1) and (2).¹⁹

Following the formalism explained above, the thickness dependence of the magnetocrystalline anisotropy in our films were obtained from FMR experiments with H rotating in the plane of the films, i.e. $\phi_H=0-360^\circ$, $\theta_H=90^\circ$. The experiments were performed at 200 K, except for the thinner samples, which were taken at 150 K to ensure that the samples are completely magnetized at the resonance field. The FMR spectra show a single Lorentzian line in all cases, except for thinner CSD films (see Figure 5). In this case two broad overlapped lines precludes the accurate analysis of their resonance field, so we excluded these samples from the discussion.

The angular dependence of $H_r(\phi_H, \theta_H=90^\circ)$ is shown in Figures 6 and 7. All samples show a clear biaxial anisotropy with the easy axis along the $\langle 110 \rangle$ direction of STO (the diagonal directions of the (001) substrate), and the hard axis coinciding with the $\langle 100 \rangle$ directions of STO (the sides of the substrates), which is in agreement with previous reports^{20,21}. Note that contrary to magnetization, in a FMR experiment the maximum and minimum of H_r mark the hard and easy magnetization axis directions, respectively. The fitting to Eq. (1) and (2) is also shown as continuous lines over the experimental data. To improve the accuracy of the fitting, the values of the saturation magnetization were obtained from the experimental $M(H)$ measurements in each sample, at the same temperature as the FMR experiments. Also the g -factor was set to $g = 2.0$, as generally observed in bulk

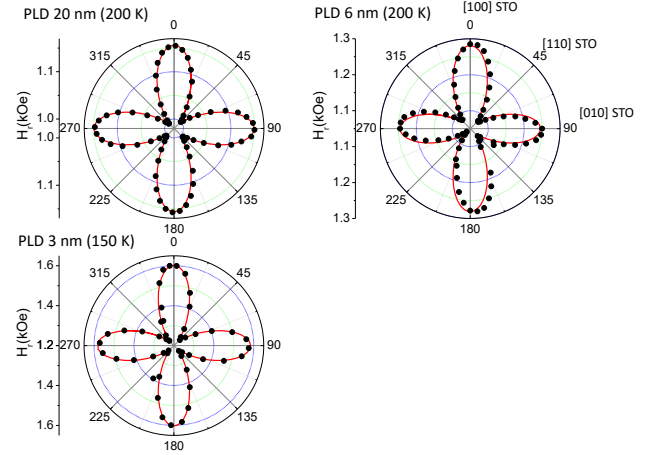


FIG. 6: In-plane angular dependence ($\phi_H=0-360^\circ$, $\theta_H=90^\circ$) of the PLD films resonance field, H_r . The spectra were acquired at 200 K, except for the thinnest sample that was taken at 150 K to ensure a good magnetization of the sample. The continuous lines correspond to the best fit numerically obtained from Eq. 1 and 2 (see text).

$\text{La}_{0.7}\text{Sr}_{0.3}\text{MnO}_3$ ^{22,23}.

The anisotropy constants obtained from the fittings are listed in Table I. All PLD films, irrespective of their thickness, are characterized by a biaxial anisotropy constant $K_4^{IP} \approx 2 \text{ kJ/m}^3$, plus an order of magnitude smaller uniaxial anisotropy K_u . The existence of these two anisotropy terms was previously reported from magnetization measurements in LSMO under tensile strain by several authors^{1,20,24,25}. The monoclinically distorted unit cell of LSMO results from a different rotation pattern of the MnO_6 octahedra along the $\langle 110 \rangle$ axis ($a^+a^-c^0$). This produces an important difference in the magnitude of the orbital overlap along the equivalent $\langle 110 \rangle$ easy axis directions, introducing the extra uniaxial anisotropy term. We also identified from this analysis an important out of plane anisotropy constant K_{out} . This term may have its origin in the contribution of different factors, like magnetocrystalline anisotropy^{18,26}, interface effects²⁷, domain shape²⁸, or most probably in this case, interfacial stress²⁹. Although this effect is normally neglected, we show here that it can be an appreciable contribution in epitaxially stressed films.

On the other hand, the situation is completely different in the films synthesized by CSD: the value of K_4^{IP} is much larger in these films compared to PLD, and most important, the uniaxial anisotropy term vanishes, $K_u \approx 0$. The out of plane anisotropy constant K_{out} is also much smaller than in the PLD films, reflecting a different contribution from interfacial epitaxial stress. A larger in-plane cubic anisotropy is in qualitative agreement with larger in-plane coercivity, as observed in Figure 4. However, the estimated $H_C \sim 2K_{ip}^4/M$ for these films is in the 80-200 Oe range, smaller than observed, which calls for

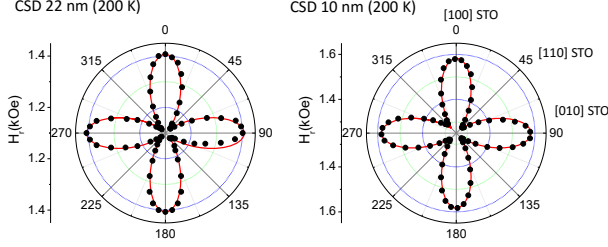


FIG. 7: In-plane angular dependence ($\phi_H=0-360^\circ$, $\theta_H=90^\circ$) of the CSD films resonance field, H_r . The spectra were acquired at 200 K. The continuous lines correspond to the best fit numerically obtained from Eq. 1 and 2 (see text).

TABLE I: Anisotropy energies obtained from the fits of the FMR curves and the corresponding saturation magnetization for the PLD and CSD films.

	t nm	K_{ip}^4 kJ/m ³	K_u kJ/m ³	K_{out} kJ/m ³	M emu/cm ³
PLD	3	2.0(2)	0.10(1)	30(3)	200
	6	1.3(1)	0.25(3)	60(6)	260
	20	2.3(2)	0.10(1)	40(4)	580
CSD	10	3.5(3)	0	10(1)	440
	25	4.5(5)	0	5.0(5)	590

further relevant effect of magnetic inhomogeneities which could act as pinning centers for domain walls³⁰. This is also consistent with the much wider FMR lines observed in CSD with respect to PLD films.

Following the argument before, the absence of K_u in CSD films indicate a similar orbital overlap along the $\langle 110 \rangle$ axis, which in turn requires an equivalent rotation of the MnO_6 octahedra along the a and b axis. The most plausible possibility is $a^+a^+c^0$ (Glazer tilt system number 16), compatible with unit cell parameters $a=b > c$ under tensile stress (tetragonal, space group $I4/mmm$) and our previous X-ray analysis (see Figure 2). The results of CSD are then consistent with an elastic deformation of LSMO, without any significant anisotropy in the octahedral tilting along the direction of the easy axis.

The arrangements of MnO_6 octahedra compatible with the analysis of the experimental FMR and XRD in epitaxial films of LSMO synthesized by PLD and CSD are

shown in Figure 8.

In summary, we have demonstrated that the characteristic in-plane uniaxial component of the magnetic anisotropy can be completely suppressed in chemically

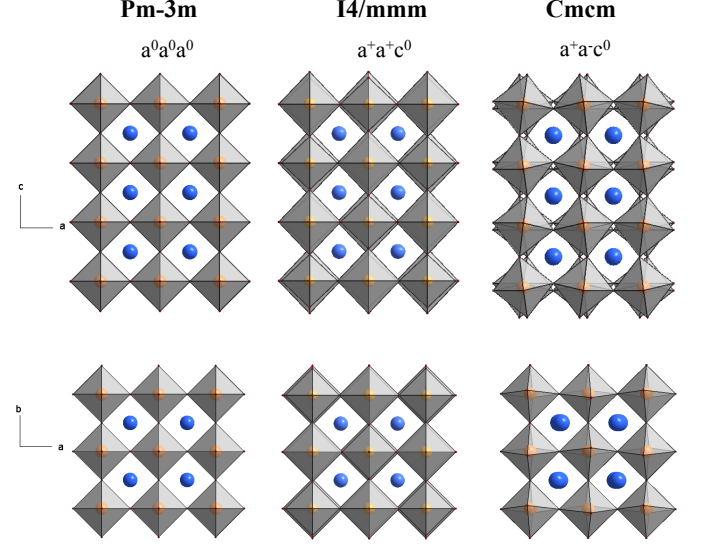


FIG. 8: Rotation pattern of the MnO_6 octahedra for the space groups adopted by the epitaxial LSMO thin-films synthesized by PLD ($Cmcm$) and CSD ($I4/mmm$). The situation for cubic STO is also included ($Pm-3m$), for comparison.

prepared thin-films of LSMO. This implies different mechanisms of octahedral rotation to accommodate the biaxial tensile stress, depending on the growth conditions. Magnetic anisotropy determines the switching and relaxation of magnetization, and therefore the results presented here are not only interesting from a fundamental point of view, but they must be considered for applications of half-metallic ferromagnet LSMO in different types of devices. Finally, we would like to remark the enormous possibilities offered by the sensitivity of FMR for the indirect study of subtle structural changes in ultrathin films, using conventional laboratory equipment.

Acknowledgments

This work was supported by the European Research Council (ERC StG-259082, 2DTHERMS), Xunta de Galicia (2012-Projet No. CP072) and by the Ministry of Science of Spain (Project No. MAT2013-44673-R). J. M. V. F. also acknowledges the same organization for an FPI grant. E.W. and J.M. thank UNCuyo Argentina for Grant No C011.

* Electronic address: f.rivadulla@usc.es

¹ A. Vailionis, H. Boschker, W. Siemons, E. P. Houwman,

- D. H. A. Blank, G. Rijnders, and G. Koster, Phys. Rev. B **83**, 064101 (2011), URL <http://link.aps.org/doi/10.1103/PhysRevB.83.064101>.
- ² A. Y. Borisevich, H. J. Chang, M. Huijben, M. P. Oxley, S. Okamoto, M. K. Niranjan, J. D. Burton, E. Y. Tsymbal, Y. H. Chu, P. Yu, et al., Phys. Rev. Lett. **105**, 087204 (2010), URL <http://link.aps.org/doi/10.1103/PhysRevLett.105.087204>.
 - ³ F. Sandiumenge, J. Santiso, L. Balcells, Z. Konstantinovic, J. Roqueta, A. Pomar, J. P. Espinós, and B. Martínez, Phys. Rev. Lett. **110**, 107206 (2013), URL <http://link.aps.org/doi/10.1103/PhysRevLett.110.107206>.
 - ⁴ J. Heidler, C. Piamonteze, R. V. Chopdekar, M. A. Uribe-Laverde, A. Alberca, M. Buzzi, A. Uldry, B. Delle, C. Bernhard, and F. Nolting, Phys. Rev. B **91**, 024406 (2015), URL <http://link.aps.org/doi/10.1103/PhysRevB.91.024406>.
 - ⁵ D. Pesquera, G. Herranz, A. Barla, E. Pellegrin, F. Bondino, E. Magnano, F. Sánchez, and J. Fontcuberta, Nature Communications **3**, 1189 (2012).
 - ⁶ L. Qiao, J. H. Jang, D. J. Singh, Z. Gai, H. Xiao, A. Mehta, R. K. Vasudevan, A. Tselev, Z. Feng, H. Zhou, et al., Nano Letters **15**, 4677 (2015).
 - ⁷ L. Marín, L. A. Rodríguez, C. Magén, E. Snoeck, R. Arras, I. Lucas, L. Morellón, P. A. Algarabel, J. M. De Teresa, and M. R. Ibarra, Nano Letters **15**, 492 (2015).
 - ⁸ R. Aso, D. Kan, Y. Shimakawa, and H. Kurata, Advanced Functional Materials **24**, 5177 (2014), ISSN 1616-3028, URL <http://dx.doi.org/10.1002/adfm.201303521>.
 - ⁹ C. Aruta, G. Ghiringhelli, V. Bisogni, L. Braicovich, N. B. Brookes, A. Tebano, and G. Balestrino, Phys. Rev. B **80**, 014431 (2009), URL <http://link.aps.org/doi/10.1103/PhysRevB.80.014431>.
 - ¹⁰ Z. Xiaofang, C. Long, L. Yang, S. Christian M., D. Shuai, L. Hui, Z. Xiaoqiang, C. Shengqi, Z. Lirong, Z. Jing, et al., Nature Communications **5**, 4253 (2014), URL <http://www.nature.com/ncomms/2014/140709/ncomms5283/full/ncomms5283.html>.
 - ¹¹ J. Suntivich, H. A. Gasteiger, N. Yabuuchi, H. Nakanishi, J. B. Goodenough, and Y. Shao-Horn, Nature Chemistry **3**, 546 (2011).
 - ¹² D. Doennig and R. Pentcheva, Scientific Reports **5**, 7909 (2015).
 - ¹³ H. Boschker, M. Huijben, A. Vailionis, J. Verbeeck, S. van Aert, M. Luysberg, S. Bals, G. van Tendeloo, E. P. Houwman, G. Koster, et al., Journal of Physics D: Applied Physics **44**, 205001 (2011), URL <http://stacks.iop.org/0022-3727/44/i=20/a=205001>.
 - ¹⁴ A. M. Glazer, Acta Crystallogr. Sect. B **28**, 3384 (1972).
 - ¹⁵ A. Vailionis, H. Boschker, Z. Liao, J. R. A. Smit, G. Rijnders, M. Huijben, and G. Koster, Applied Physics Letters **105**, 131906 (2014), URL <http://scitation.aip.org/content/aip/journal/apl/105/13/10.1063/1.4896969>.
 - ¹⁶ J. M. Vila-Figueirinho, B. Rivas-Murias, B. Rodríguez-González, O. Txoperena, D. Ciudad, L. E. Hueso, M. Lazari, and F. Rivadulla, ACS Applied Materials & Interfaces **7**, 5410 (2015).
 - ¹⁷ J. Smit and H. Beljers, Philips Res. Rep. **10**, 113 (1955).
 - ¹⁸ M. Barturen, J. Milano, M. Vázquez-Mansilla, C. Helman, M. A. Barral, A. M. Llois, M. Eddrief, and M. Marangolo, Phys. Rev. B **92**, 054418 (2015), URL <http://link.aps.org/doi/10.1103/PhysRevB.92.054418>.
 - ¹⁹ C. Vittoria, *Microwave properties of magnetic films* (World Scientific, 1993), ISBN 9781118211494.
 - ²⁰ K. Steenbeck and R. Hiergeist, Applied Physics Letters **75**, 1778 (1999), URL <http://scitation.aip.org/content/aip/journal/apl/75/12/10.1063/1.124817>.
 - ²¹ F. Tsui, M. C. Smoak, T. K. Nath, and C. B. Eom, Applied Physics Letters **76**, 2421 (2000), URL <http://scitation.aip.org/content/aip/journal/apl/76/17/10.1063/1.126363>.
 - ²² G. Alejandro, M. Otero-Leal, M. Granada, D. Laura-Ccahuana, M. Tovar, E. Winkler, and C. M. T., Journal of Physics: Condensed Matter **22**, 25602 (2010).
 - ²³ V. A. Ivanshin, J. Deisenhofer, H.-A. Krug von Nidda, A. A. Loidl, A. and Mukhin, and M. V. Balbashov, A. M. and Eremin, Physical Review B **61**, 6213 (2010).
 - ²⁴ H. Boschker, M. Huijben, A. Vailionis, J. Verbeeck, S. van Aert, M. Luysberg, S. Bals, G. van Tendeloo, E. P. Houwman, G. Koster, et al., Journal of Magn. Magnetic Mat. **323**, 2632 (2011).
 - ²⁵ M. Belmeguenai, S. Mercone, C. Adamo, L. Méchin, C. Fur, P. Monod, P. Moch, and D. G. Schlom, Phys. Rev. B **81**, 054410 (2010).
 - ²⁶ B. Cullity and C. Graham, *Introduction to Magnetic Materials* (Wiley, 2011), ISBN 9781118211496.
 - ²⁷ S. Ikeda, K. Miura, H. Yamamoto, K. Mizunuma, H. Gan, M. Endo, S. Kanai, J. Hayakawa, F. Matsukura, and H. Ohno, Nature Materials **9**, 721 (2010).
 - ²⁸ F. Vidal, Y. Zheng, P. Schio, F. Bonilla, M. Barturen, J. Milano, D. Demaille, E. Fonda, A. De Oliveira, and V. Etgens, Physical Review Letters **109**, 117205 (2012).
 - ²⁹ E. Sallica Leva, R. Valente, F. Marttínez Tabares, M. Vázquez Mansilla, S. Roshdestwensky, and A. Butera, Physical Review B **82**, 144410 (2010).
 - ³⁰ H. Kronmüller and M. Fähnle, *Micromagnetism and the microstructure of ferromagnetic solids* (Cambridge University Press, 2003), ISBN 9781118211495.